A novel minimally invasive and reproducible large animal ischaemia-reperfusion-infarction model: methodology and model validation

Charlene Pius, Barbara Niort, Emma J. Radcliffe, Andrew W. Trafford*

Division of Cardiovascular Science, School of Medical Science, Faculty of Biology Medicine and Health, University of Manchester, Manchester Academic Health Science Centre, United Kingdom

* Corresponding
Andrew.W.Trafford@manchester.ac.uk
3.24 Core Technology Facility
46 Grafton Street
Manchester
M13 9NT
United Kingdom
+44 161 275 7969

A novel minimally invasive and reproducible large animal ischaemia-reperfusion-infarction model: methodology and model validation

Abstract

Ischaemic heart disease remains a leading cause of premature mortality and morbidity. Understanding the associated pathophysiological mechanisms of cardiac dysfunction arising from ischaemic heart disease and the identification of sites of novel therapeutic intervention requires a preclinical model that reproduces the key clinical characteristics of myocardial ischaemia, reperfusion and infarction. Here we describe and validate a refined and minimally invasive translationally relevant approach to induce ischaemia, reperfusion and infarction in the sheep. The protocol uses clinical cardiology devices and approaches and would be readily adopted by researchers with access to standard fluoroscopic instrumentation. In addition to being minimally invasive, the major refinements associated with the described methodology are the implantation of an intracardiac defibrillator prior to coronary engagement and use of an antiarrhythmic medication protocol during the procedure. These refinements lead to a reduction of intraoperative mortality to 6.7 %. The model produces key characteristics associated with the 4th Universal Definition of Myocardial Infarction including electrocardiographic changes, elevated cardiac biomarkers and cardiac wall motility defects. In conclusion, the model closely replicates the clinical paradigm of myocardial ischaemia, reperfusion and infarction in a translationally relevant large-animal setting and the applied refinements reduce the incidence of intraoperative mortality typically associated with preclinical myocardial infarction models.

2

Introduction

25   Cardiovascular diseases, mainly ischaemic heart diseases (IHD), are the leading cause of
26   mortality in the United Kingdom[1, 2] and worldwide[3]. Coronary artery disease (CAD) is one of
27   the most important causes of IHD[4] and is characterised by a reduction in the volume of
28   perfusion to the heart (i.e., ischaemia) or even its complete cessation (i.e., infarction)[5-7]. Acute
29   myocardial infarction (MI) is defined as myocardial necrosis in the context of myocardial
30   ischaemia, which can be transmural, involving all three layers of the heart (endocardium, mid-
31   myocardium, and epicardium) or non-transmural, typically sparing the epicardium[5-11].
32   Classically, non-transmural MI present clinically with non-ST segment elevation (NSTEMI) on
33   the electrocardiogram (ECG) are treated primarily with anti-platelet treatment, peri-
34   interventional anticoagulant treatment, and coronary angiography with a view to
35   revascularization within 72h[11]. Transmural MI are associated with ST segment elevation
36   (STEMI) on the ECG and are treated with primary percutaneous coronary intervention
37   (PPCI)[12]. Complications following MI include ventricular arrhythmias (VA)[13, 14] and heart failure
38   (HF)[15], which can manifest early or late[15-17]. VA can occur in the form of ventricular tachycardia
39   (VT)[14, 18] or ventricular fibrillation (VF). These life-threatening complications necessitate
40   increased research to identify novel therapeutic targets that may ultimately alter prognosis
41   following MI and ultimately this necessitates translationally relevant animal models.

42   When studying a disease, especially the precise molecular aspects of dysregulation, the
43   animal model should ideally be as clinically relevant as possible. Occluding a coronary artery
44   in an experimental animal can induce a reaction comparable to an acute MI caused by
45   atherosclerosis or thromboembolic events. Most of the current small (mouse or rat)[19] and large
46   (pig, sheep or dog) mammal models of cardiac dysfunction from ischaemia consist of the
47   permanent ligation of the LAD[20-24] (for review see[25, 26]). Whilst they are reliable models for
48   inducing tissue damage and HF, they do not accurately reflect the clinical setting occurring as
49   a result of a reperfusion of the occluded vessel during PPCI. Other models use intracoronary
50   injections of thrombogenic material causing a permanent occlusion and therefore, in the same
51   way, do not reflect the typical clinical situation. Importantly, the reperfusion phase may also
52   be associated with cardiac dysfunction known as ischaemia-reperfusion injury (IRI) including
53   arrhythmias, myocardial stunning and vascular obstruction[27]. None of these potential sequelae
54   occur in models of total and permanent occlusion.

55   The development of percutaneous transluminal coronary angioplasty balloon catheters to treat
56   coronary atherosclerotic stenosis has led to the creation of less invasive ischaemia-
57   reperfusion animal models. However, all these models still present with a low survival rate[20,
58   28, 29], predominantly owing to arrhythmic death or low cardiac output state[28]. This high mortality
59   rate is at odds with key elements of the 3R's principles of animal research[30-32] (Reduction;
60   Refinement and Replacement), making the establishment of a large mammal MI model more
61   challenging.

62   The heart of large animals shares many electrophysiological and contractility similarities to
63   humans, which is why modelling cardiac diseases in these species generally better reflects
64   human pathologies and thus drug and interventional effects than in small animals[33].
65   Additionally, large animal models also allow for the implementation of minimally invasive
66   approaches and use of clinical grade materials and devices thus conferring an inherent
67   refinement aspect of 3R's considerations. Canine and porcine models using balloon occlusion

68   of coronary arteries already exist. However, both models present limitations. Studies suggest
69   that the vascular architecture of the porcine and canine heart differs from that of a human
70   heart, and hence may be less representative of the remodelling that occurs in a human with
71   ischaemic heart disease. Specifically, when compared to human, pig and sheep, rodent and
72   canine hearts are known to have a greater collateral network which can affect the ability to
73   form a predictable infarct size[34-36]. Furthermore, pig models are associated with a high rate of
74   sudden death caused by ventricular arrhythmias following MI (reviewed in[37]). Lastly, an
75   additional logistical consideration is that husbandry can become very difficult as pigs grow
76   rapidly to large size. The ovine heart is one of the closest to the human, and therefore is
77   accepted as a good pre-clinical animal model for cardiovascular research[38]. A clear scientific
78   protocol for the experimental induction of ischaemia/infarction-reperfusion injury and study of
79   STEMI in sheep is lacking. It is essential to develop comprehensive, reproducible, reliable
80   protocols and criteria for knowledge and skill transfer, as well as to ensure that investigations
81   can be replicated with minimal animal suffering to ensure good proximity to the clinical
82   scenarios the in vivo modelling is attempting to reproduce.

83   Here, we have developed a minimally invasive large mammal ischaemia/infarction-reperfusion
84   model in sheep, which is more clinically relevant, with a considerably lower mortality rate
85   (6.7%) than other previously reported large animal models. To that end, we refined a
86   prophylactic intra-operative anti-arrhythmic drug protocol and added a surgical step involving
87   the implantation an internal cardiac defibrillator to assist with rapid defibrillation of ventricular
88   arrhythmias.
89

Results

Defining a model of infarction-reperfusion large mammal

A total of 28 female Welsh Mountain sheep aged ~18 ± 6 months weighing 38 ±1.2 kg were used in this study. Following carotid cannulation, a 6F JR4 guide catheter was advanced down the 6F haemostatic sheath to reliably engage the left coronary ostium. After left coronary artery angiography, the balloon was successfully placed below the second diagonal branch of the LAD (supplementary figure 1). Only 2 of the 28/30 sheep died following MI induction from intractable ventricular fibrillation. Total mortality was 6.7 % all occurring intraoperatively before reperfusion.

Using a minimally invasive coronary angiographic technique, the infarct was created by inflating an intra-coronary balloon for 90 minutes to occlude blood flow followed by reperfusion. Both occlusion and reperfusion were confirmed by angiography. In order to validate the model, we set out to achieve the key criteria set out in the 4th universal definition where MI is defined as myocardial necrosis in the context of myocardial ischaemia resulting in an elevation of a cardiac biomarker such as cardiac troponin I (cTnI)[39] with at least one value above the 99th percentile upper reference limit. The diagnosis of MI requires additional criteria, including at least one of the following: (1) clinical symptoms of ischaemia including chest discomfort; (2) electrocardiographic (ECG) ischaemic features such as the development of new changes in the ST and T segment (ST-T) or new left bundle branch block (LBBB); (3) new pathological Q waves; (4) imaging evidence of reduced cardiac wall contractility; and/or (5) evidence of an intracoronary thrombus visualised via angiography or on autopsy[40, 41]. Specific objective assessment of chest discomfort is clearly impossible to achieve in animal models, however each of the remaining four criteria are assessable with readily applicable methods or investigations. We will, in turn, consider each of the assessable 4th Universal Definition criteria achieved using the minimally invasive model of STEMI presented here.

Temporal changes in serum cTnI

In this model, cTnI serum levels were easily and rapidly evaluated[42] using whole blood samples and a point-of-care device (see Methods; upper limit of detection 50 ng/ml). Measurements were made at various stages during the procedure (Fig 1). At baseline, all animals had near-zero values. Following the inflation of the angioplasty balloon, we observed an elevation in a cTnI ($p < 0.0001$), displaying the typical rise and fall pattern seen in STEMI patients[43-46]. The cTnI levels rose significantly during reperfusion (1.2 ± 1ng/ml; $p < 0.01$) and continued to rise at 30 minutes post-reperfusion (27.4 ± 3 ng/ml; $p < 0.0001$) with a peak observed at a measurement time of 90 minutes post-reperfusion (46 ± 1.8 ng/ml; $p < 0.0001$) when compared to baseline (0.03 ± 0 ng/ml). The levels started to decline by day 2 to 4 (21.5 ± 3 ng/ml; $p < 0.0001$ vs baseline) with a further decline after 1 week (0.6 ± 0.2ng/ml; $p < 0.01$ vs baseline) and returning to baseline values by week 3 (0.03 ± 0.0 ng/ml) and remaining low until the end of the study (week 8; 0.01 ± 0.0 ng/ml) (Fig. 1).

128

129 **Fig. 1 - cTnI measurements.** cTnI
130 measurements at baseline, intraoperatively and
131 on day 2 - 4, 1 - 1.5 weeks, 3 weeks and 8
132 weeks demonstrating the expected rise and fall
133 pattern seen in MI. *N*, baseline= 28; pre-
134 occlusion = 28; immediate reperfusion = 27; at
135 30 mins post-reperfusion = 28; 90 mins post-
136 reperfusion = 28; Days 2 - 4= 28; Weeks 1 -
137 1.5= 20; Week 3 = 9; Week 8 = 10. **** p <
138 0.0001 ** p < 0.01 vs baseline; #### p < 0.0001
139 vs 90 minutes post-reperfusion by Kruskal-Wallis
140 test.

141

142

143
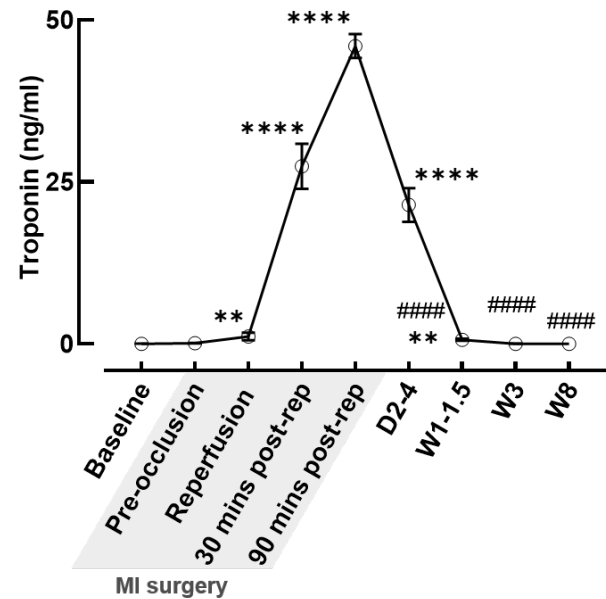
144 **Electrocardiographic changes following myocardial ischaemia-reperfusion injury**
145 The intention with this model was to create an ST segment elevation MI thus most closely
146 resembling the clinical cohort of patients being treated with PPCI. The ST segments started
147 to rise upon coronary occlusion (0.07 ± 0.02 mV) with a statistically significant increase seen
148 on reperfusion (0.13 ± 0.03 mV; $p < 0.0001$) compared to baseline (0.02 ± 0.00 mV). ST
149 segment normalisation was already evident at the end of surgery (0.05 ± 0.01 mV; $p < 0.05$
150 vs reperfusion) (Fig. 2a and b). The dynamic pattern of these ST segments supports the
151 diagnosis of MI[41, 47]. Intraoperative ventricular arrhythmias requiring intracardiac defibrillation
152 were observed in 8 of 27 animals.

153 The T wave amplitude peaked on reperfusion (0.19 ± 0.03 mV; $p < 0.05$) compared to baseline
154 (0.13 ± 0.03 mV) with a gradual return to near normal values by the end of surgery (0.12 ±
155 0.02 mV; $p < 0.01$ vs reperfusion) (Fig. 2c and d). T peak amplitude increment could be a
156 consequence of interstitial hyperkalaemia from myocardial ischaemia[42,43].

157 We also took the opportunity to calculate the T-peak Tend interval, which is suggested as a
158 measure of transmural dispersion of repolarization[40,41]. Upon coronary occlusion, the Tpeak-
159 Tend interval more than doubled (83 ± 11 ms vs 37 ± 2.3ms ; $p < 0.001$) with maximal
160 prolongation seen on reperfusion (110 ± 16ms; $p < 0.0001$) declining by the end of surgery
161 (96 ± 16 ms; $p < 0.001$) whilst remaining prolonged compared to baseline (Fig. 2d and e).
162

6
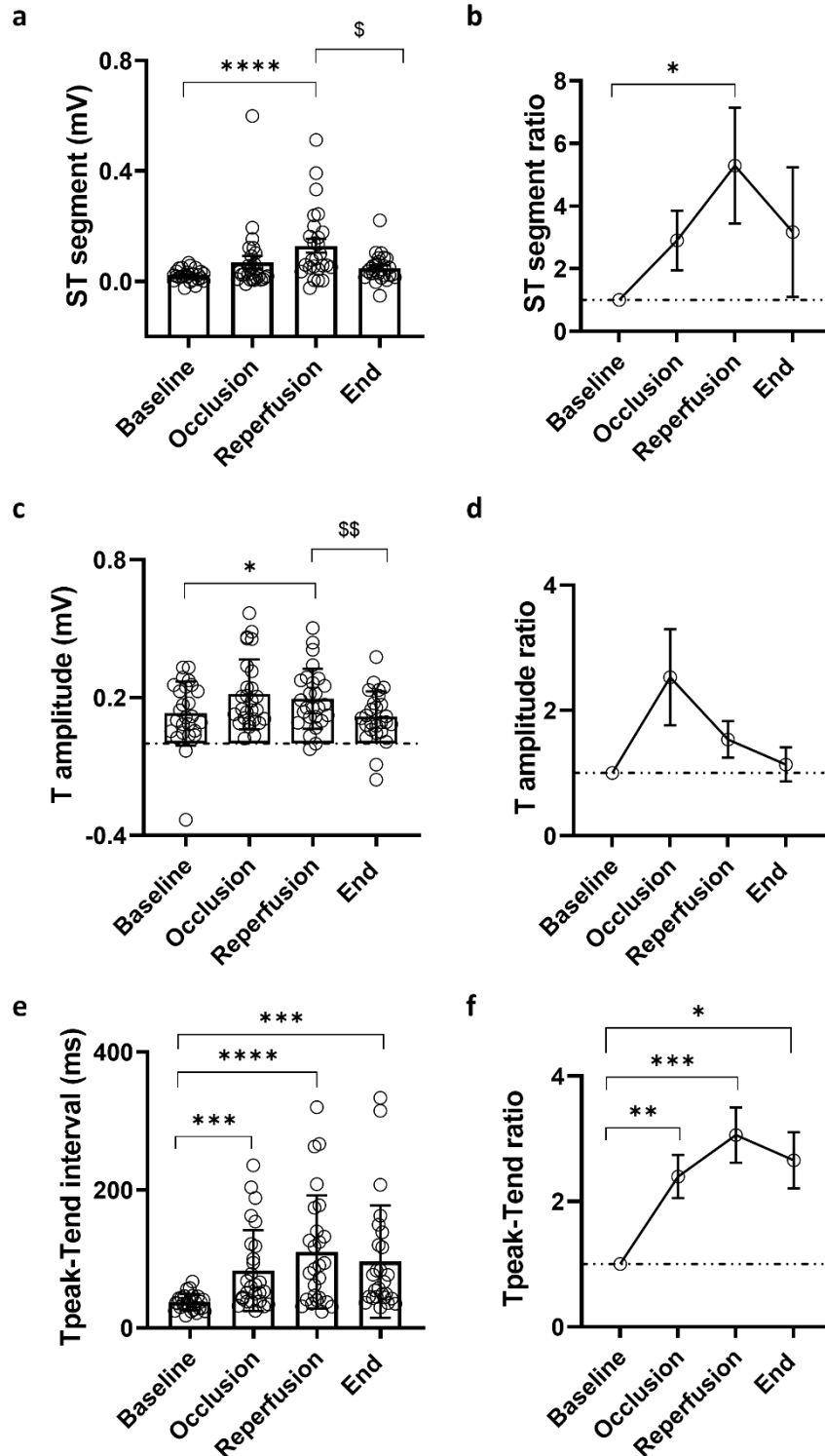
Fig. 2 Electrocardiographic changes following ischaemia-reperfusion injury. ST segment changes as **a**, absolute measurements and **b**, difference in height compared to baseline. T wave amplitude changes as **c**, absolute measurements and **d**, ratio compared to baseline measurements. Tpeak-Tend interval changes as **e**, absolute values and **f**, ratio values compared to baseline. N, baseline = 25 - 27, occlusion = 25 - 27, reperfusion = 25 - 26, end = 25 -26. **** $p < 0.0001$, *** $p < 0.001$, ** $p < 0.01$, * $p < 0.05$ vs baseline, \$\$ $p < 0.01$, \$ $p < 0.05$ vs reperfusion by mixed effects model analysis and RM one-way ANOVA.

172 **Change in cardiac contractile function and planimetry**

173 Left ventricular ejection fraction (EF) was estimated at intervals as described in the methods
174 section. Pre-surgery EF was 73 ± 1.4 % and declined following MI being 58 ± 2.1% at 1 – 1.5
175 weeks ($p < 0.0001$), 60 ± 3.1% ($p < 0.05$) and 52 ± 1.7 % at 8 weeks post MI ($p < 0.0001$)
176 demonstrating a 21% decline in EF compared to baseline ($p < 0.0001$) (Fig. 3a). While the
177 final EF value at 8 weeks was higher than those mentioned in other studies[44], the total
178 reduction in EF of 21% was bigger than the 14% described in a previous study[45]. We also
179 measured fractional shortening (FS), as a measure of contractility and this parameter also
180 declined from pre-surgery levels of 39 ± 1.1% to 30 ± 1.4 % at 1 – 1.5 weeks and 27 ± 1.1%
181 at 8 weeks respectively following MI. (Fig. 3b, $p < 0.0001$).
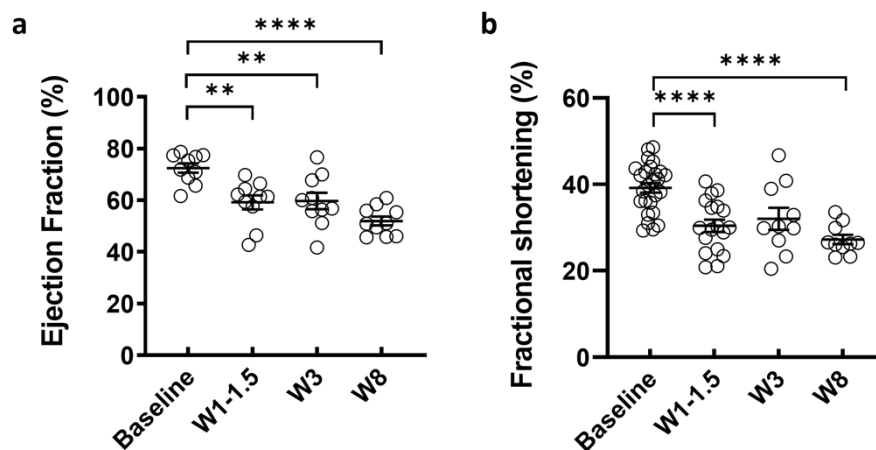
182
183 **Fig. 3 – Echocardiographic evaluation of LV systolic function**. Measurements of **a**, EF
184 and **b**, FS from baseline to week 8. *N*, Baseline= 25, W1 - 1.5 = 17, W3= 10, W8 = 10. **** p
185 < 0.0001, ** p < 0.01, compared to baseline, by mixed effects model analysis.

186
187
188 After an MI it is known that LV remodelling involves changes in wall thickness in both infarcted
189 and non-infarcted regions[48-50]. We first evaluated the wall thickness of the infarcted region in
190 comparison to the non-infarcted LV wall. Here, we present the results as the fraction of the
191 change in wall thickness at the infarcted site when compared to the non-infarcted site on the
192 same acquisition plane in systole and diastole. This was done to reduce the effect of variations
193 in the acquisition plane, particularly at the distal LV level where landmarks were less clear.

194 At mid-LV level, there were no statistically significant changes in the wall thickness in diastole
195 (Fig 4a) or systole (Fig 4b) following MI, which was likely due to the more apical infarct location.
196 Conversely, at the distal-LV level, where the infarct would be more pronounced, an increase
197 in wall thickness was noted at week 1-1.5 and week 3 in both diastole and systole compared
198 to baseline (Fig 4c). In systole, there was an increase in wall thickness which was maintained
199 from 1 – 1.5 to 8 weeks post MI (Fig 4d). These changes are likely due to the occurrence of
200 eccentric hypertrophy in the non-infarcted wall, thinning of the infarcted wall segments or a
201 combination of both. These differences were more pronounced in systole as the infarcted
202 segment is akinetic and unable to thicken adequately compared to the hyper-contractile non-
203 infarcted segment[51]. These wall thickness changes further support the finding of regional wall
204 motion abnormality, which further fulfils criteria set out in the Universal Definition of MI.
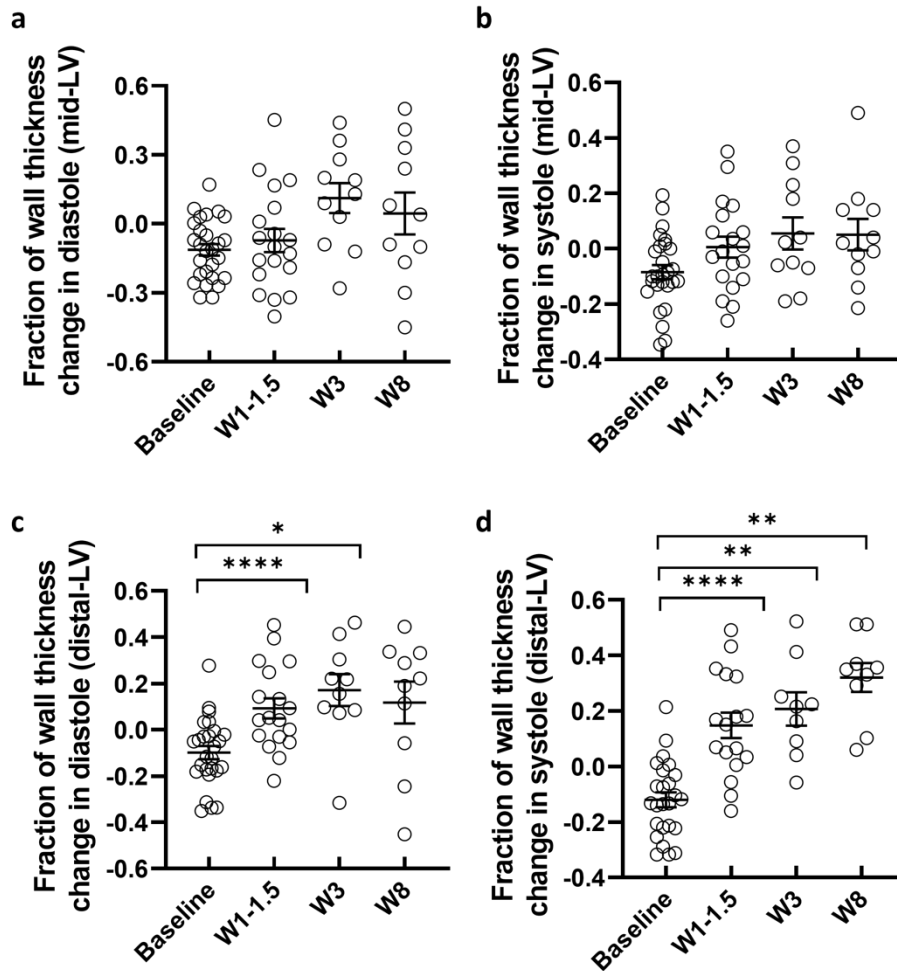
Fig. 4 – Fraction of wall thickness change. Wall thickness changes at mid-level in (**a**), diastole, and (**b**), systole. *N*, baseline=27, W1-1.5=19, W3=11, W8=11. Wall thickness changes at distal-LV level in diastole (**c**) and systole (**d**) *N*, baseline=25, D3=8, W1-1.5=17, W3=9, W8=9. ****$p < 0.0001$, **$p < 0.01$, *$p < 0.05$ by mixed effects model analysis.

Gross morphology and infarct size.

The transient occlusion of the LAD after the second diagonal branch resulted in a well-defined area of infarction detectable at all three-time intervals despite varying appearance reflecting the acute, proliferative and maturation stages of scar formation (Fig. 5a, b and c). At 8 weeks, infarcts were more easily measured due to the presence of visible white area of scar tissue. The infarcts were less well visually defined after 3 days and 1.5 weeks. The infarct was best seen in a cross-sectional image, revealing the intra and transmural nature of scar tissue distribution. Planimetry was used to assess the size of the infarct from the anterior surface of the LV. The average size of an infarct was 4.7 ± 1 cm^2. However, the infarct frequently extended around the apex into the posterior wall, making it difficult to accurately determine the infarct size using this measuring approach..

The variability in infarct size is consistent with the variable infarct size seen in humans. No correlation between infarct size and troponin levels (Fig. 5e) were observed but this is likely related to the limitations on both infarct size measurement and the upper limits of detection of the point of care cTnI assay (50ng/ml).

9
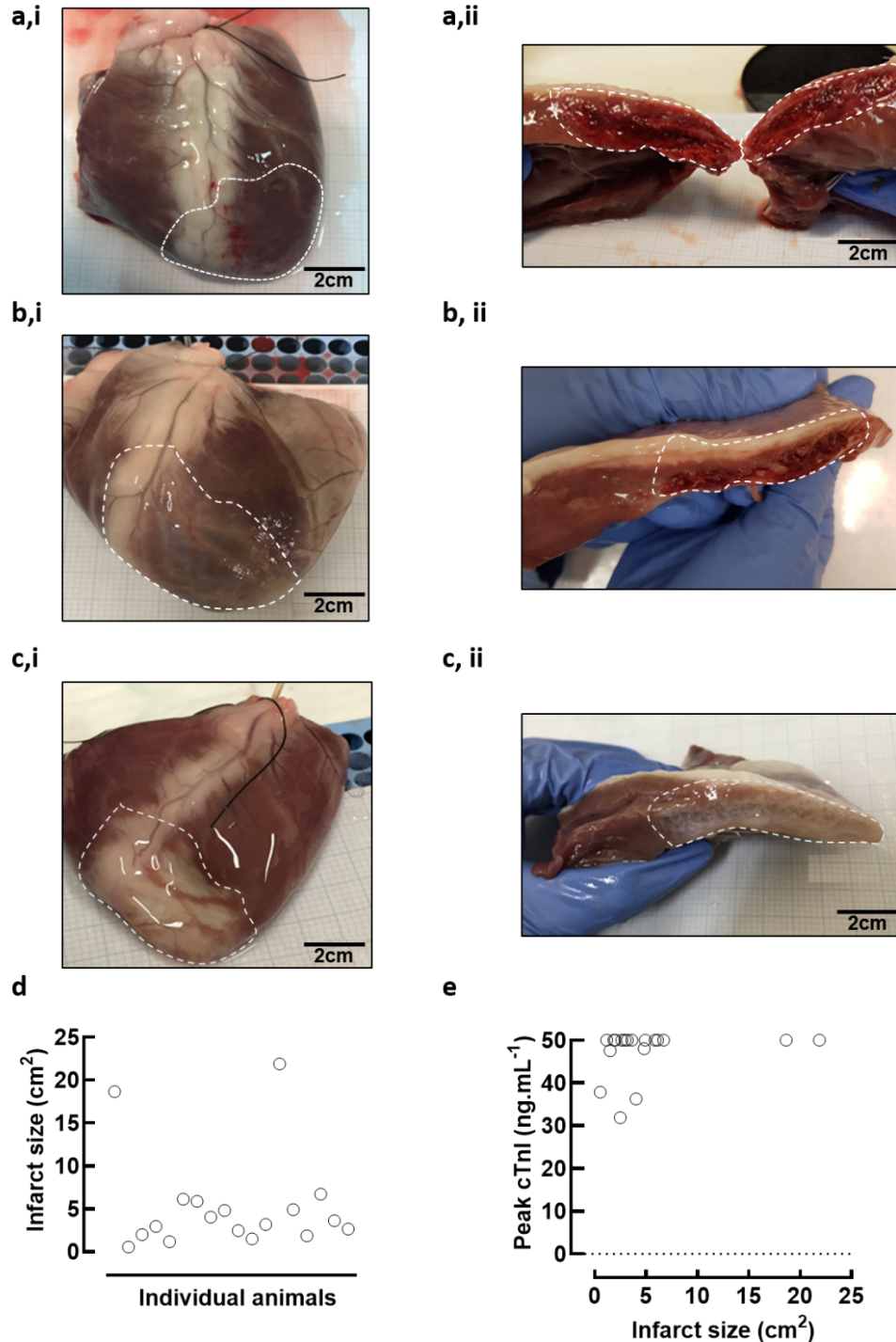
Fig. 5 – Infarcts at 3 days, 1.5 weeks and 8 weeks. Images of infarcts at **a**, 3 days, **b**, 1.5 weeks and **c**, 8 weeks as **i**, whole ventricle images and **ii**, LV cross-sectional images demonstrating different appearances in the infarct over time. The scale bar is shown in black. **d,** Infarct sizes from all animals at 3 days, 1.5 weeks and 8 weeks. **e**, The peak troponin value plotted against the infarct size with no relationship seen (*N*=26). Relationship are determined by simple linear regression.

Discussion

We aimed to create a refined minimally invasive ischaemia/infarction-reperfusion model of myocardial infarction with improved survival outcomes. It was critical that our model survived to the specified time points of 3 days, 1.5 weeks, and 8 weeks in order to assess the temporal evolution of the acute, latent, and chronic phases following a myocardial infarction. In order to achieve this, the experimental protocol was refined with specific measures to reduce the mortality rate previously described in the literature[28] including the inclusion of prophylactic anti-arrhythmic medications[47, 52, 53] and the implantation of an internal cardiac defibrillator. Using this surgical and medication protocol, we successfully created reproducible infarcts and reduced procedural mortality. Importantly, the model fulfils the key criteria of the 4th universal definition of MI demonstrating i) the rise and fall of a cardiac biomarker (cTni), ii) electrocardiographic changes in the ST-T segment, iii) echocardiographic evidence of wall motion abnormality and iv) evidence of scar/infarct on the heart.

During the occlusion period, we observed cardiac repolarization abnormalities in the form of ST-T segment changes. The presence of ST elevation indicates a transmural infarction, which affects the heterogeneity of the ionic properties of cardiac cells from the epicardial, myocardial, and endocardial layers[54, 55]. It is debateable as whether the repolarisation abnormalities are more reflective of transmural injury or the baso-apical position of the injury[56].

We also observed changes in contractile function and wall thickness over the temporal evolution of the MI. It is known that, during the post infarct remodelling phase, the infarcted segment undergoes thinning and expansion. The apico-anterior segments are particularly vulnerable to this as they are the thinnest segments with the greatest curvature[57-60]. This is accompanied by hypertrophy of the non-infarcted region[57-62], which may serve as a temporary compensatory mechanism. The hypertrophy occurs in response to increased wall stress as a consequence of the infarcted segment[61]. This is often not enough to restore the original function, as we have demonstrated here. In fact, this eccentric hypertrophy often contributes to worsening dilatation during remodelling[60], which may explain to the deterioration in LV function observed at 8 weeks.

There was large inter-animal variability in infarct size with a coefficient of variation of 104%. This is likely due to the inter-animal LAD anatomical variations in the D2 bifurcation point and the limitations of the infarct measurement method. In an effort to standardize the approach, we aimed to occlude the LAD after the D2 bifurcation. However, the variability in coronary anatomy, particularly of the LAD vessel which has been previously described in sheep is likely to have contributed to this[45]. We aimed to achieve an anterior-apical infarct involving ~ 25% of the LV. In some animals, the point of D2 bifurcation was quite proximal and would affect more than the intended area of myocardium. Whereas in other animals, the D2 branch followed a similar course to the LAD towards the apex potentially co-supplying the intended infarct territory.

Finally, we demonstrated a lower rate of attrition and improved mortality rate compared to existing work[20, 28, 29] with the refinements in our experimental protocol. The models have survived the planned experimental time periods successfully allowing the temporal evolution of MI to be studied at an *in vivo* level and will allow future cellular and tissue studies.
Finally, we demonstrated that this model is clinically relevant due to similarities with existing STEMI patients undergoing PPCI reperfusion treatment. As a result, this model will allow for

11

284   a better understanding of the pathological evolution following MI and will help in the research
285   of new therapeutic targets that may improve patient outcomes post MI. Furthermore, with
286   further refinement, this model may be able to reflect a translatable HF model of ischemic
287   cardiomyopathy following STEMI and could be used to select cardioprotective medications to
288   protect STEMI patients from reperfusion damage.
289

290   The refinement aspects developed in this study encompassed the inclusion of a prophylactic
291   intra-operative antiarrhythmic strategy including the use of amiodarone, lidocaine and atenolol
292   and the use of an implantable cardiac defibrillator. Whilst approximately one-third of animals
293   developed ventricular arrhythmias requiring defibrillation, our overall intra-operative mortality
294   was reduced to 6.7%. This compares favourably to previous studies[20, 26, 29, 37] and provides a
295   methodological approach that is easily applied to other large animal ischaemia reperfusion
296   studies.
297
298

Methods

Ethical statement. All procedures involving the use of animals were performed in accordance with the United Kingdom (UK) Animals (Scientific Procedures) Act, 1986 and European Union Directive 2010/63. Local ethical approval was obtained from the University of Manchester Animal Welfare and Ethical Review Board. Reporting of animal experiments was in accordance with the ARRIVE guidelines 2.0 [31].

Animal. Experiments were performed on naïve adult (~18 months) female Welsh Mountain sheep. Animals were not randomised as this study focused on model development and did not contain a sham-operated arm as all statistical comparisons were paired to pre-surgical values in the same animals. Animals were group housed, fed hay and water *ad libitum*, and maintained on a 12-hour light/12-hour dark cycle for at least 1 week prior to surgical intervention.

Myocardial infarction surgery. In line with all experiments necessitating the use of general anaesthetic, animals were fasted overnight to prevent the risks of gastric distension but had unrestricted access to water. The full step by step protocol is available in Extended Methods Online Supplement. Induction of anaesthesia was achieved using a combination of isoflurane, (5% vol/vol) Santa Cruz Biotechnology, USA), Nitric Oxide (50%vol/vol) and O_2 (50% vol/vol at a flow rate of 5 L/min) administered via facemask. The depth of anaesthesia was confirmed by loss of the corneal blink reflex[63]. To facilitate the passage of the endotracheal tube into the trachea, lignocaine local anaesthesia spray (Xylocaine, Astra Zeneca, UK) was applied topically, reducing vocal cords and pharynx spams and tracheal intubation with a curred endotracheal tube (8-10 mm). The cuffed endotracheal tube was then inflated to ensure a sealed circuit, avoid anaesthetic leakage, and prevent secretions and gastric contents from entering the lungs. The tube was then connected to a mechanical tidal ventilator (Zoovent, UK) and ventilation performed at a rate of 15 breaths/min. The maintenance of anaesthesia was achieved using an isoflurane concentration ~3% mixed with O_2 (4L/min). The following parameters were constantly monitored during the surgery: i) the depth of anaesthesia was monitored by assessing the corneal blink reflex, ii) arterial blood pressure an electronic sphygmomanometer (Cardell Veterinary Monitor 9402, Sharn, USA) placed on the shaved tail base, iii) arterial O_2 saturation (kept above 95%) using a doppler pulse oximeter (Nonin Medical, Inc., USA) placed on the tongue or on the shaved ear and, iv) the electrocardiogram was monitored using a five-lead continuous ECG (EMKA Technologies) digitised to a computer at a sampling rate of 1kHz (iOX2, EMKA Technologies).

In order to correct for any blood loss during the surgery, an intravenous (IV) maintenance fluid (0.9% NaCl, Baxter, USA) was administrated via an 18 to 22-gauge cannula (BD Microlance™, UK) positioned in the lateral saphenous vein from the right posterior limb at a constant flow rate over the course of surgery. This venous line was also used as a route for the administration of intravenous drugs (Fig. 6) via a coupled three-way tap.

Meloxicam (0.5 mg.kg^{-1} subcutaneously; Metacam®, Boehringer Ingelheim, Germany) and amoxicillin (20µg.kg^{-1} Betamox®, intramusculalrly Norbrook, UK; or amoxicillin sodium, intramuscularly, Bowmed Ibisqus Ltd, UK) were used to provide analgesia and antibiosis. The surgery was carried out in two stages under aseptic conditions.

Implantation of the internal cardiac defibrillator (ICD)

345 The first stage consists of the implantation of an internal cardioverter defibrillator (ICD) device
346 in order to allow prompt cardioversion of any sustained intra-operative ventricular arrhythmias
347 and record the electrical cardiac function in the post-operative period. In detail, the animal was
348 positioned in left lateral recumbency. A sterile field was prepared by shaving the wool over the
349 right cervical region and cleansing with iodine (iodinated povidone 7.5 % Videne, UK). An ~ 8
350 cm skin incision was made in the jugular groove and bunt dissection was used out to expose
351 the jugular vein. Once adequately freed of attached fascia, 2.0 silk sutures (Ethicon, USA)
352 were loosely placed proximally and distally. Further blunt dissection was then carried out to
353 identify the carotid artery, which runs deeper alongside the vagus nerve. The carotid artery
354 was then freed from the vagus nerve using blunt dissection and 2.0 silk anchoring sutures
355 were placed loosely at the proximal and distal points of the artery (Fig. 6 a and b).

356 After tying off the proximal part of the jugular vein, a small incision was made into the vein and
357 maintained open using a vein pick to allow the insertion of an ICD lead (Medtronic USA) The
358 single chamber defibrillator lead comprises, from proximal to distal, an electrode to be
359 anchored within the myocardium, and bifurcated (in a single coil lead) or trifurcated (in dual-
360 coil lead) header connector pins. The connectors consist of one pace-sense IS-1 (or IS-4)
361 connector, and one or two DF-1 (or DF-4) high voltage connectors[64]. Consequently, the active
362 fix right ventricular (RV) lead was carefully advanced to the apex of the RV under fluoroscopic
363 guidance (BV Pulsera, Philips, Netherlands).

364 The correct lead tip position was assessed prior to fixation in the RV by connecting the lead
365 to an electrophysiological analyzer (Medtronic 209o Analyser; Medtronic Inc) and assessing
366 three intraoperative electrocardiographic parameters: (i) the pacing threshold (i.e., the lowest
367 pulse amplitude at which the heart can still be paced); (2) intracardiac potential (R-wave
368 amplitude), and (3) lead impedance (300 - 1500Ω)[65, 66]. Satisfactory elad positioning was
369 confirmed by a combination of i) pacing threshold < 1V, ii) R wave amplitude > 6mV and lead
370 impedance < 1500 Ω. Once satisfactory lead and pacing parameters were confirmed the ICD
371 lead was connected to the ICD can and secured in position using 2.0 silk suture where it
372 entered the jugular vein. The latter minimizes the risk of dislodgment. Any excess lead length
373 was wrapped in loose loops around the ICD can before being positioned inside a
374 subcutaneous pocket created above the jugular distally to the original incision towards the
375 right shoulder. The pocket was securely closed using Vicryl 2.0 sutures. To avoid inappropriate
376 shocks, the device was configured to only detect the following zones: VT, VF and Fast VT
377 zones). In this ovine model, inappropriate detection has been observed as high sinus
378 tachycardia rates and T wave over-sensing, therefore the device was programmed purely for
379 detection. The defibrillator is then set to emergency mode for the duration of the surgery,
380 allowing for fast defibrillation when intra-operative ventricular arrhythmias.
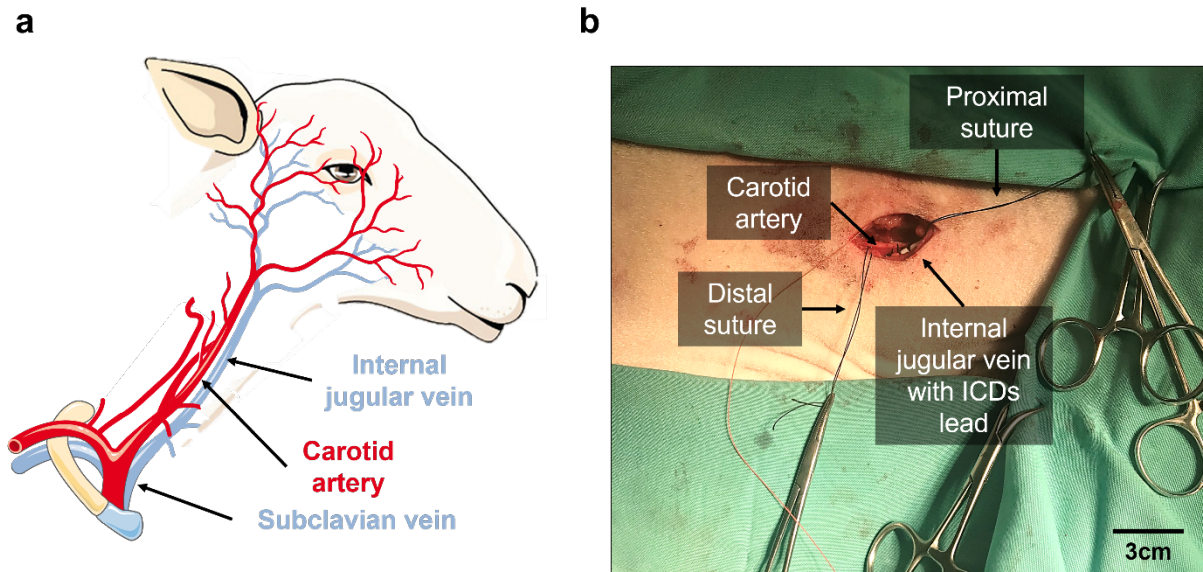
Fig. 6 – Intraoperative images of surgery. a, Schematic of the isolated vessels in the sheep neck. **b,** Picture of the surgical site (right side of neck) shaved and cleaned, showing the incision with sutures placed on the distal and proximal aspect of the carotid artery.

Induction of myocardial infarction

Access to the arterial circulation was obtained via the carotid artery which was identified at the start of the surgery. The originally placed 2.0 suture at the proximal end of the vessel was secured. Using the Seldinger technique[67], the carotid was punctured with a 14-gauge cannula. A soft curved tip guidewire (Abbott, USA) was then inserted through the cannula and advanced into the arterial lumen. The guidewire was securely held in place whilst the cannula was withdrawn. A 12 cm 6Fr haemostatic introducer sheath (Abbott, USA) was passed over the guidewire into the lumen. The guidewire was withdrawn, leaving the introducer sheath in the vessel. The sheath was loosely secured with a suture placed into the surrounding soft tissue to avoid displacement due to carotid pulsation. 10,000 IU of heparin sodium (Wockhardt Ltd., India) was injected as a bolus, and the IV maintenance fluid at the right posterior limb cannula was switched for one containing 0.9% NaCl IV infusion at 10 IU heparin per mL. The medication protocol including the prophylactic anti-arrhythmic drug regime is demonstrated in Fig. 7.

A 6Fr Judkins right (JR4) catheter (Runway, Boston Scientific Quincy, USA) was preloaded with a 0.35mm J tip wire (Cordis, USA or Abbott, USA) and advanced through the introducer sheath to the aortic valve level under fluoroscopic guidance leading with the J-tipped wire. The wire was then removed, and the left main stem (LMS) was engaged with a 50:50 mix of radiocontrast agent (Visipaque™, GE Healthcare Inc., USA; 270 mg/mL) and 0.9% NaCl solution injected through the sheath catheter. A coronary angiogram was performed to opacify the left coronary system. The left coronary system consisted of the left main stem which bifurcates into the left circumflex (LCx) and left anterior descending (LAD) coronary artery, also known as the left homonymous in sheep [17,61–63]. The LCx supplies the posterior and lateral free walls of the left ventricle (LV) whereas the LAD supplies the anterolateral, septal and apical walls of the LV[62,64,65]. Upon identification of the LAD, a hydrophilic 0.014-inch guidewire (Abbott, USA) was advanced to the distal LAD. Depending on the calibre of the vessel, an

413 appropriately sized intracoronary balloon catheter (Apex Monorail or Emerge™, Boston
414 Scientific, MA, USA) was advanced and positioned within the LAD, after the second diagonal
415 branch (D2; Supplemental Figure SI). The length of the intracoronary balloon used was 20 –
416 40 mm with a width ranging from 2 - 2.75 mm depending on the coronary anatomy and calibre
417 determined empirically during coronary angiography using the Judkins catheter diameter as a
418 guide. The balloon catheter was inflated to the specified recommendations using an Indeflator
419 (BasixCompak inflation device, Merit Medical, USA) with a repeat coronary angiogram
420 thereafter confirming complete occlusion of flow distal to the inflated balloon (Fig. 6;
421 Supplemental Figure SI). The balloon remained inflated for 90 minutes occluding blood flow
422 distal to the balloon, thus creating the infarct.
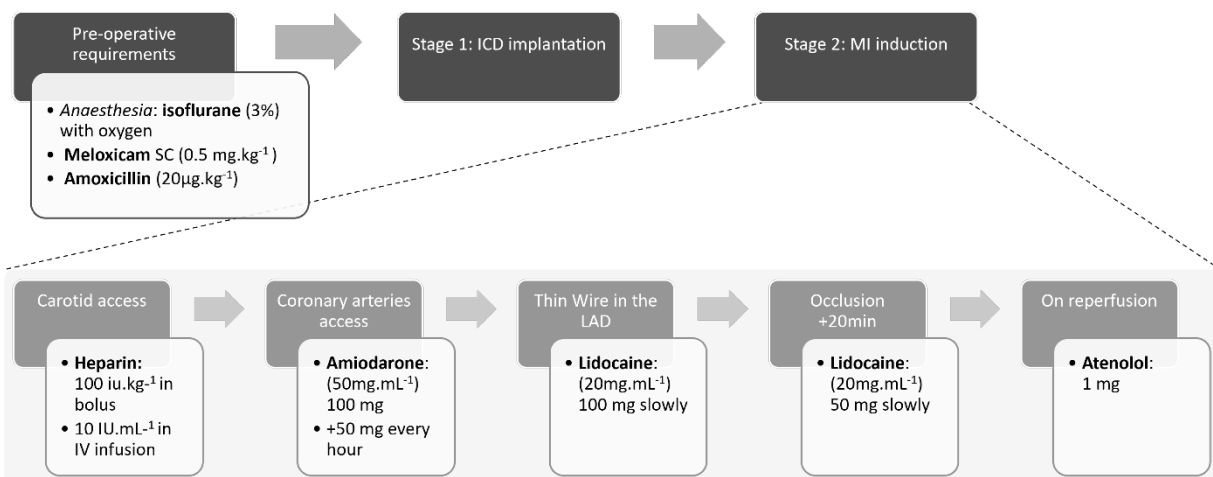
423
424 **Fig. 7 - Drug protocol for MI induction surgery**. Diagram of the timings of medications
425 administered during MI induction surgery. Internal cardiac defibrillator (ICD) device; anterior
426 descending artery (LAD).

427 ECG and intracardiac electrogram (via ICD) parameters were continuously monitored for the
428 presence of ST elevation, T wave changes and conduction abnormalities and ventricular
429 arrhytmias. ST segment changes were usually observed within minutes of coronary occlusion
430 with evidence of additional ventricular activity seen approximately 30 - 40 minutes into the
431 occlusion. These ranged from the occasional ventricular ectopic (VE) beats to VF requiring
432 defibrillation. In the event of a persistent ventricular arrhythmias such as VT or VF, the animal
433 would be promptly defibrillated via the ICD to terminate the arrhythmia.
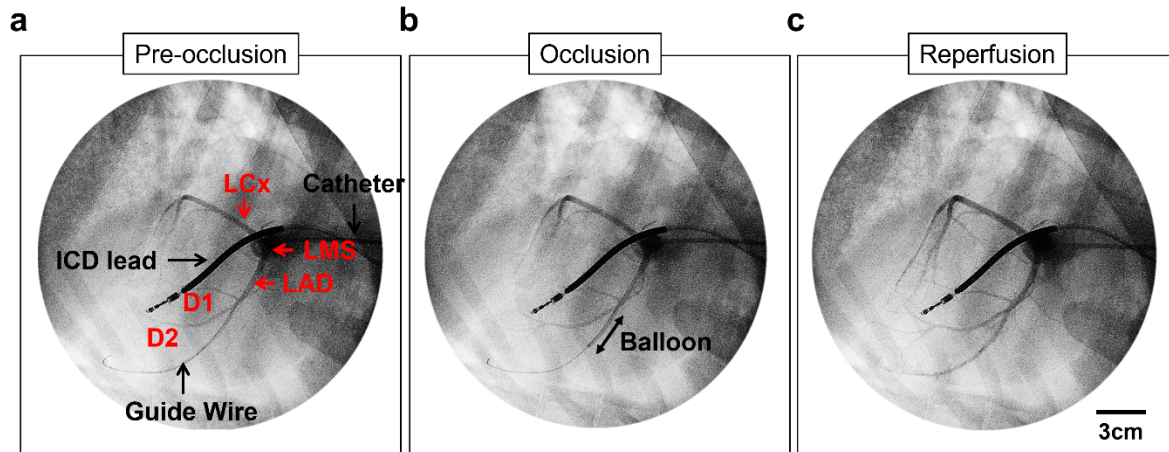
Fig. 8 - Fluoroscopic images during MI induction surgery. a, Angiogram of the left coronary system showing the left main stem (LMS) bifurcating into the left anterior descending (LAD) and left circumflex (LCx) coronary artery. The ICD lead is also seen within the RV. **b,** Repeat coronary angiography with an inflated intracoronary balloon occluding flow distal to the balloon. **c,** Confirmation of the correct reperfusion of the heart. D1 and D2, diagonal branches. RA, right atria. RCA, right common coronary artery. Videos in supplemental material (Supplemental material SI)

90 minutes after inflation the balloon was deflated and coronary blood flow distal to the occlusion site was confirmed with a repeat coronary angiogram Fig. 8. The intracardiac equipment and sheath were removed. The distal carotid artery was tied off with a 2.0 silk suture. The wound was closed in three layers, closing the muscular fascia, the subdermal tissue and finally the cutaneous layer. During the wound closure, the isoflurane concentration was gradually reduced from 3% to 0%. The endotracheal tube was left in place until the animal showed the signs of a rejection reflex (i.e., swallow or cough). The recovery from anaesthesia was closely monitored for evidence of respiratory distress and arrhythmias. The IV catheter was left in place until the animal was fully awake to allow immediate IV access. Once the animal was alert and all vital signs were within normal range, it was placed in a single housed post-operative recovery pen in full sight and communication with its peers and was given access to food and water.

The animal was closely monitored during the recovery period. It was considered fully recovered from anaesthesia when visibly alert, standing and having urinated. After 24h of post-operative recovery housing the animal was returned to group housing. No further intervention was carried out for at least three days to ensure complete recovery from surgery as well as to allow the ICD lead to settle in its intracardiac position. Animal weight, well-being and wound healing were monitored regularly to ensure adequate post-operative recovery.

***In vivo* assessments.** To assess the evolution of various clinical and cellular parameters over time following MI, the animals were randomly divided into three groups: 3-day MI, 1 - 1.5 week MI, and 8 week MI. As shown in Fig. 9, *in vivo* measurements were performed at baseline, post-operatively, and at the endpoint. There were two types of evaluations performed: full assessments and expedited assessments. The full in vivo assessment included measurement of weight and blood pressure, recording of electrocardiograms (ECG), imaging using transthoracic echocardiography (TTE), blood sampling, and external interrogation of an intracardiac device once implanted. The expedited assessment only involved blood sampling and the device interrogation.
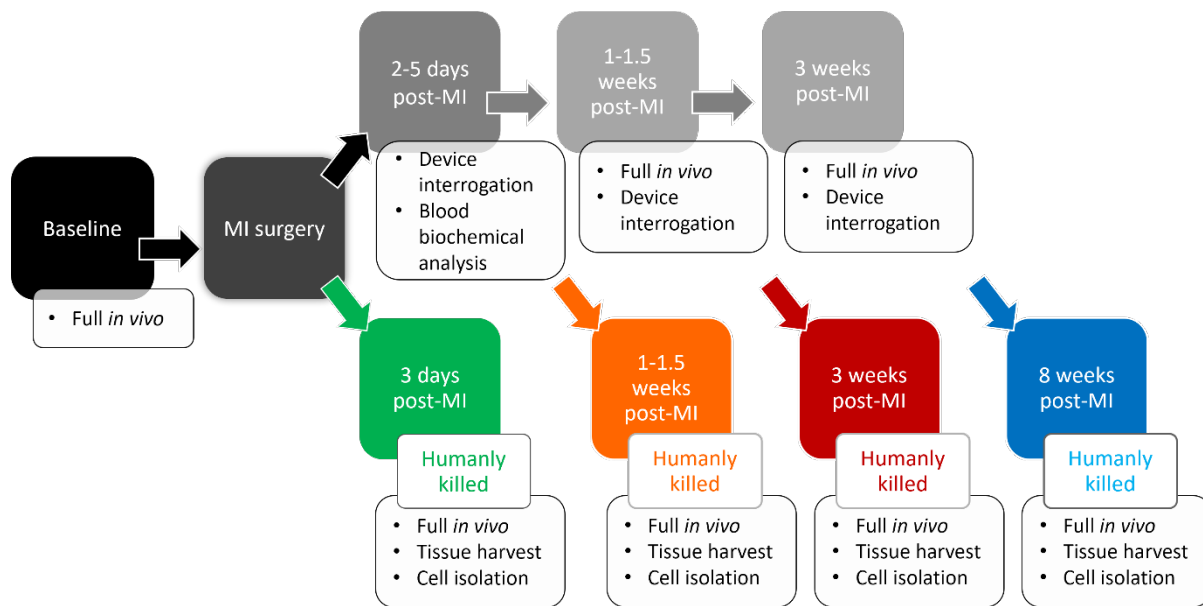
Fig. 9 - *In vivo* schedule for 8 week, 3 week, 1-1.5 week and 3 day MI animals. The full *in vivo* assessment included measurement of weight and blood pressure, recording of electrocardiograms, imaging using transthoracic echocardiography, blood sampling, and external interrogation of an intracardiac device once implanted.

Blood sampling

Blood was collected pre-operatively, at multiple time points intraoperatively (carotid artery access, pre-occlusion, 30min post-reperfusion and 90min post-reperfusion), at 2 - 5 days, 1 - 1.5 weeks and 8 weeks. Venous blood sampling was performed preferably from the right jugular vein with the animal gently restrained using a sterile aseptic non-touch technique. Alternative sampling sites included the left jugular vein or cephalic veins. The skin was shaved and aseptically cleansed before sampling. Amongst the blood parameters evaluated were whole blood cTnI (VetScan i-STAT, Abaxis, UK) as a marker of myocardial necrosis along with a full biochemistry profile (Skyla VB1 Analyser, Woodley, UK). The full profile is shown in Supplement (Supplemental Table 1). The cTnI was tested using a point-of-care testing system, which provided a result within 10 minutes.

Transthoracic echocardiography

In the same seated position, under gentle restraint, transthoracic echocardiography (Vivid, GE Healthcare,USA) was performed with the probe positioned on the right side of the chest with the right forelimb lifted, providing access to the thorax. Image quality was optimised by shaving the chest and using an ultrasound transmission gel (Aquasonic, Germany) for better contact. As limited views were available, parasternal short (SA) and long (LA) axis views were obtained to allow evaluation of the cardiac structure and function. For adequate visualization of the LV walls and endocardial borders, the apical views (2, 4 and 5 chamber views) would have been ideal. However, the anatomical position of the heart and wide sternum in sheep makes this difficult to obtain[56]. The SA-mid view was taken below the mitral valve level where the papillary muscles were visible. The SA-distal view was the most distally obtainable short axis image of the LV to visualize the apex and adjacent region. In humans, regional wall motion

499   abnormalities can be assessed using a 17-segment ECHO model where the LV walls are
500   divided into 17 segments which can be correlated to the blood supply[57,58].

501   For the analysis, images were exported and converted from DICOM to JPEG format using
502   Microdicom Viewer (Microdicom, Bulgaria). The JPEG files were opened in Fiji ImageJ
503   (National Institutes of Health, USA) and multiple measurements were taken.
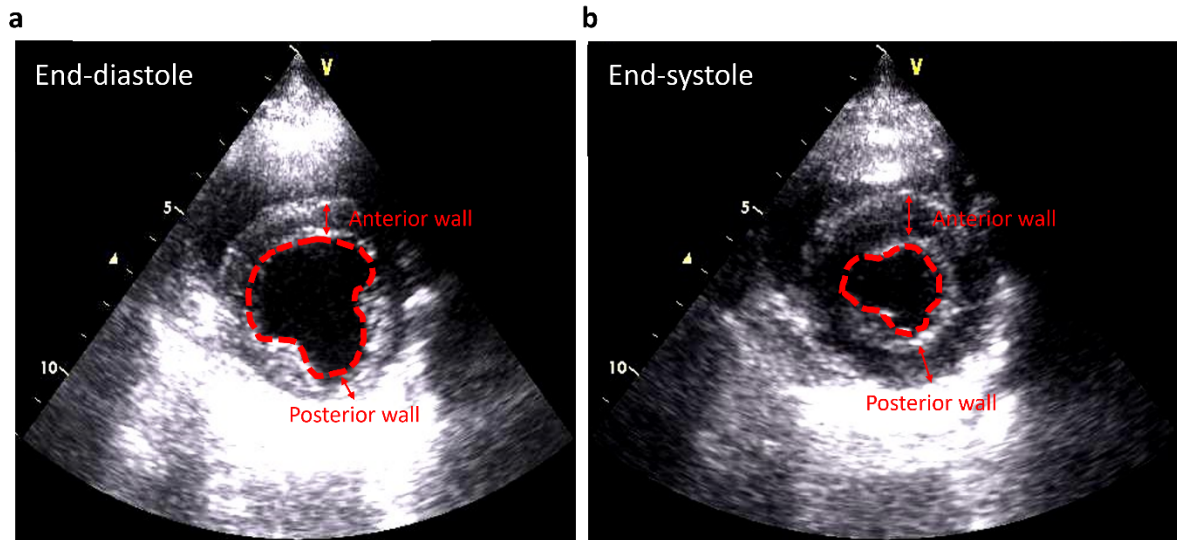
504
505   **Fig. 10 – Measurements from ECHO SA-mid views.** Frames from the LV short axis views
506   at mid-level in diastole **a,** and systole **b,** with the anterior and posterior wall thickness
507   measurement sites (marked by red arrow) as well as the LV cavity area measurement
508   (outlined in red-dotted line) shown.
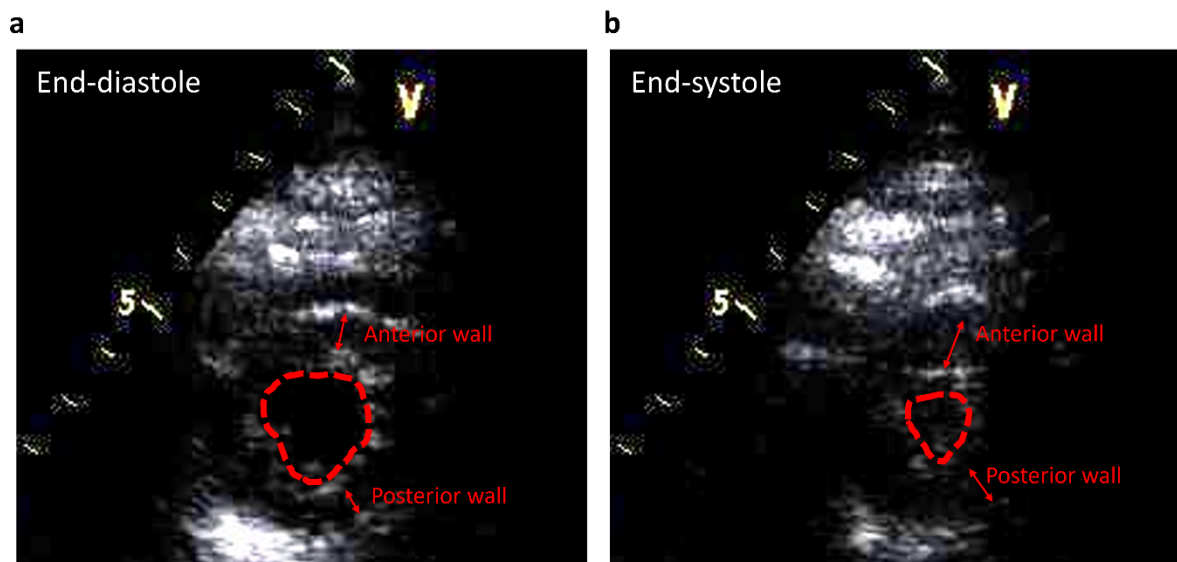
509
510   **Fig. 11 – Measurements from ECHO SA-distal views.** Frames from the LV short axis views
511   at distal-level in diastole **a,** and systole **b,** with the anterior and posterior wall thickness
512   measurement sites (marked by red arrows) as well as the LV cavity area measurement
513   (outlined in red-dotted line) shown.

514   In the SA-mid and SA-distal images, the anterior wall thickness measurement represented the
515   infarcted region, and the posterior wall thickness represented the non-infarcted region (Fig.
516   10 and Fig. 11). Prior to the surgery, measurements were also taken from these identical sites

19

to serve as baseline values. The fraction of wall thickness change (FWTC) was calculated using Equation 1 to determine the difference in wall thickness between the infarcted and the non-infarcted region. In order to assess the fractional area change (FAC) as a measure of contractile function, the LV cavity area (Fig. 10 and Fig. 11) was also measured at mid and distal LV levels in systole and diastole and calculated using Equation 2.

$$Fraction\ of\ wall\ thickness\ change = \frac{(Non\ infarcted - Infarcted)}{Non\ infarcted}$$

Equation 1   Fraction of wall thickness change

$$Fractional\ area\ change = \frac{(Diastolic\ area - Systolic\ area)}{Diastolic\ area} \times 100$$

Equation 2   Fractional area change

From the parasternal long axis (PLAx) images, the interventricular septal (IVS) thickness, LV end diastolic (LVEDD) and systolic diameter (LVESD) as well as the LV posterior wall (LPW) thickness were measured in diastole and systole as shown in Fig. 12. Due to the limited obtainable views in the sheep, estimating the LV function was challenging particularly in the presence of an apical infarct. Therefore, an adaptation of the simplified Quinones equation produce by MD Math available from the Canadian Society of Echocardiography[59] was used deriving an estimated ejection fraction (EF) from the LVESD, LVEDD and an apical contractility estimate seen from the SA-distal views using Equation 3. In this equation, the K value (Table 1) represented the apical contractility. Additionally, fractional shortening (FS) was also calculated as another measure of contractile function using Equation 4 and expressed as a percentage.
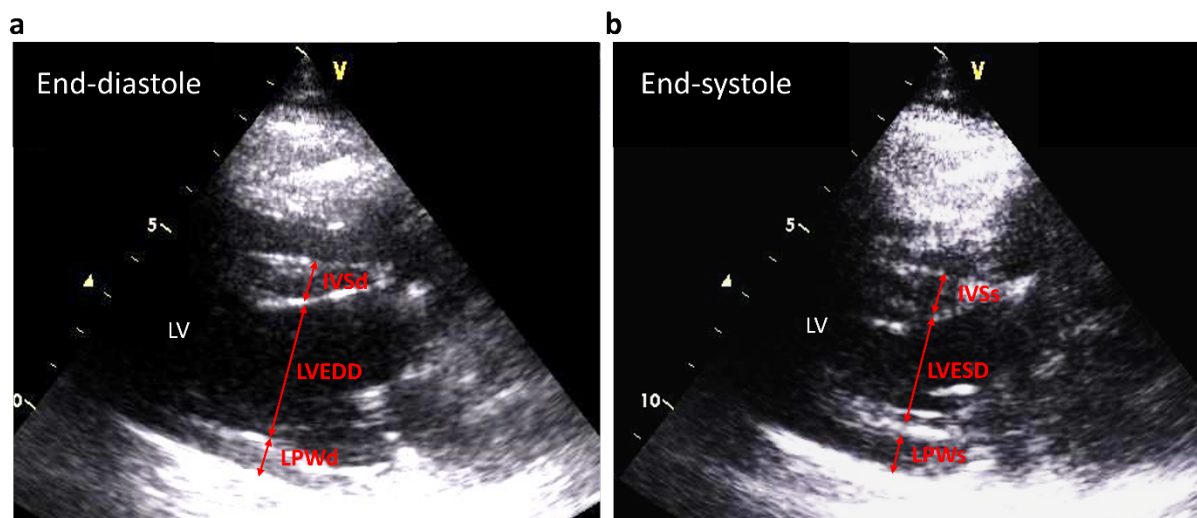
Fig. 12 – Measurements from ECHO PLAX views. Frames from the PLAX views in diastole **a,** and systole **b,** with the interventricular septal thickness (IVS) (yellow arrows), LV end diastolic (LVEDD) and systolic diameter (LVESD) (blue arrows) and left posterior wall thickness (LPW) (orange arrows). For IVS and LPW measurements, the letter *s* or *d* at the end denote measurements taken in systole or diastole, respectively.

548

Apical contraction	K value (%)
Normal	+10
Hypokinetic	+5
Akinetic	0
Dyskinetic	-5
Apical aneurysm	-10

549 **Table 1 - K values.** Apical contractility measurements expressed as percentages, used in
550 Equation 2.4

551

$$Ejection\ Fraction\ (EF) = \frac{LVEDD^2 - LVESD^2}{LVEDD^2}\ X\ 100 + K$$

553
554 **Equation 3   Ejection fraction**

555
556

$$Fractional\ shortening\ (FS) = \frac{LVEDD - LVESD}{LVEDD}\ x\ 100$$

558
559 **Equation 4   Fractional shortening**

560
561 **Electrocardiography**
562 Surface electrocardiograms were recorded at intervals. Peri-operative ECG recordings (EMKA
563 Technologies, USA) were performed in the seated position using 5 surface electrodes in an
564 orthogonal arrangement on shaved and cleaned sites to allow better contact. The identical
565 electrode position is used again intraoperatively but the animal is laid on its left-hand side
566 during surgery. Upon connecting electrodes, the animal was allowed some time to settle thus
567 minimizing any potential stress-related ECG changes[60] or motion artefacts. A 10-minute ECG
568 was then recorded through IOX software (EMKA Technologies, France)

569 For the analysis, the files were opened in ECG Auto (EMKA Technologies, France) and
570 converted text file (*.TXT) format to allow the files to be opened on Labchart (AD Instruments,
571 UK). The recordings were smoothed and filtered to reduce noise and breathing artefacts using
572 a 21-point (Bartlett) window and a 2 Hz high pass or 50 Hz notch filter.

573 The software generated multiple averaged traces consisting of 10 consecutive beats over the
574 1-minute selected recording period where intervals could be manually selected.
575
576 **Euthanasia.** The humane killing of MI sheep was carried out as per the approved regulated
577 procedure and schedule 1 protocol in accordance with ABPA regulations with an anaesthetic
578 overdose (pentobardbitone sodium, 200 mg/kg intravenously) followed by permanent
579 cessation of circulation. Humane killing was performed at three predetermined timepoints post
580 MI: 3 days, 1.5 weeks and 8 weeks post-MI.

581 **Statistical analysis.** All data is expressed as the mean ± SEM. Statistical analysis was
582 performed using Prism 7 (GraphPad Software, San Diego, California). Data were first tested
583 for normality using Shapiro-Wilk, Kolmogorov-Smirnov, Anderson-Darling, and D'Agostino-
584 Pearson omnibus in GraphPad Prism. Where data were not normally distributed, data were
585 transformed using, natural log, Log_{10}, reciprocal, square root or exponential depending on
586 skew[67]. Normally distributed data were analysed using the t-test, one way ANOVA, repeated
587 measures one way ANOVA and mixed effects model analysis. Where data was not normally
588 distributed despite transformation, an equivalent non-parametric test was used. The
589 relationship between two variables was determined using simple linear regression and the
590 correlation was evaluated using Pearson's correlation (provided by the r value). Data was
591 considered significant if the p value was < 0.05 and is described in the text.
592
593
594

Data Availability

The data supporting this manuscript are available from the corresponding author on reasonable request.

Acknowledgements

Ethics Statements

The authors have no financial or competing interests to declare

Author Information

AWT conceived the experiments and secured all funding. CP led the model development and performed all analyses. All authors contributed to surgical and in vivo procedures. CP, BN and AWT drafted the manuscript. All authors approved manuscript contents.

621 **Step by step guide**

622 **MATERIALS**

623 **Animals**

624 • Young, treatment naïve Welsh Mountain sheep (aged ~18 ± 6 months) with an average
625 weight 38.5 ± 1.2kg
626 • Group housed, fed hay and water ad libitum and maintained in a 12 hour light/12 hour
627 dark cycle for a minimum of 1 week prior to surgical intervention.

628

629 **Reagents**

630 • Lignocaine local anaesthesia throat spray (Xylocaine, Astra Zeneca, UK)
631 • x3 Heparin 10,000 IU in 10 ml vials (Wockhardt, UK)
632 • Contrast medium – Ionohexol (Omnipaque 300, GE Healthcare, USA)
633 • x3 Sodium chloride 0.9% 500mls and 1000mls (Baxter, USA)
634 • Prophylactic antibiotics (Amoxicillin 15 mg kg^{-1}) (Norbrook, UK)
635 • Prophylactic analgesia meloxicam (0.05mg kg^{-1}) (Norbrook, UK)
636 • Amiodarone (Hameln, UK)
637 • Lidocaine (Hameln, UK)

638

639 **Premedication and Anaesthesia**

640 • 1-chloro-2,2,2-trifluoroethyl difluoromethyl ether (isoflurane, Santa Cruz
641 Biotechnology, USA)
642 • Oxygen and nitrous oxide (50:50) mix (BOC Healthcare, The Linde Group, Germany)
643 • Cone face mask rubber large

644

645 **Equipment**

646 • Hypodermic needle variable sizes 18, 20, 22G (BD Microlance, UK)
647 • 5ml, 10ml, 20ml and 50ml syringe (BD Plastipak, UK)
648 • IV infusion set (CareFusion, USA)
649 • 14G & 20G cannula (BD Venflon, USA)
650 • Blood pressure cuff and machine (Mindray, Australia)
651 • Pulse oximeter sensor (Mindray iMEC8 Vet Manuals, Mindray Bio-Medical Electronics
652 Co., China)
653 • 5 lead ECG cable with crocodile clips and recording equipment, IOX software (EMKA
654 Technologies, France)
655 • iSTAT Vetscan Hand held analyser and cTni cartridges (Abaxis, UK)
656 • Ultrasound transmission gel (Aquasonic, Germany)
657 • GE Vivid 7 echocardiography machine with 5S cardiac transducer (General Electrics,
658 USA)
659 • Skyla VB1 Biochemistry analyser (Woodley, UK)
660 • C-arm fluoroscopy machine (BV Pulsera Mobile C-arm, Philips, UK)

661

662 **Intubation** (see Fig. 13 – Typical surgical equipment. a, Intubation equipment. b, Surgical
663 tray.
664 • Miller laryngoscope blade size 4
665 • Stiff endotracheal stylet

24

666 • Cuffed endotracheal tube (size 8.5 to 10; J.A.K Marketing, UK)

667 • 20mL syringe (BD Plastipak, UK)

668 • The ribbon to tie the ET tube in place

669 • Bag valve mask

670

671 Monitoring and anaesthesia

672 • Anaesthetic machine (Zoovent, UK)

673 • Five-lead electrode cable with leg strips

674 • Electrocadiogram monitoring (IOX software, EMKA technologies,USA)

675 • Pulse oximeter sensor (Mindray iMEC8 Vet Manuals, Mindray Bio-Medical Electronics
676 Co., China)

677 • Blood pressure cuff sized as tail cuff and BP recording equipment (Mindray, Australia)

678

679 Surgical site preparation, generic operative equipment & operator preparation

680 • Sheep clippers

681 • Iodinated povidone 7.5% (Videne, UK)

682 • Sterile drapes

683 Surgical tray (see (see Fig. 13 – Typical surgical equipment. a, Intubation equipment. b,
684 Surgical tray.)

685 • Gallipot

686 • 2.0 Vicryl sutures (Ethicon,USA)

687 • 2.0 Silk sutures (Ethicon,USA)

688 • 2.0 Monocryl sutures (Ethicon,USA)

689 • Sterile gauzes

690 • Internal cardiac defibrillator

691   ο Generator (Medtronic, USA)

692   ο Right ventricular active fixation defibrillator leads (DF1 or DF4) (Boston
693   Scientific, Medtronic, USA)

694   ο ICD compatible programmer with analyser cable and header (*e.g.* Medtronic
695   2090, Medtronic, Minnesota, USA)

696   ο PSA cables

697 • MI Induction

698   ο 14G cannula (BD Venflon,USA)

699   ο 12cm 6Fr haemostatic introducer sheath (Abbott Medical, UK), containing the
700   sheath, a dilator and a mini-guidewire

701   ο 6F JR4 Guide catheter (Runway, Boston Scientific, USA)

702   ο Haemostasis valve (Honor,Merit Medical, USA)

703   ο Indeflator (balloon inflation device) with pressure monitor (BasixCompak
704   inflation device, Merit Medical, USA)

705   ο 50ml syringe (BD Plastipak, USA)

706   ο Intracoronary balloon catheter, variable sizes 2.2 to 2.75mm diameter, 20-
707   40mm length (Apex Monorail, Boston Scientific, MA, USA)

708   ο 0.35 J tipped guide wire (Cordis, USA)

709   ο 0.0014 intracoronary guide wire (Abbott, USA)

710
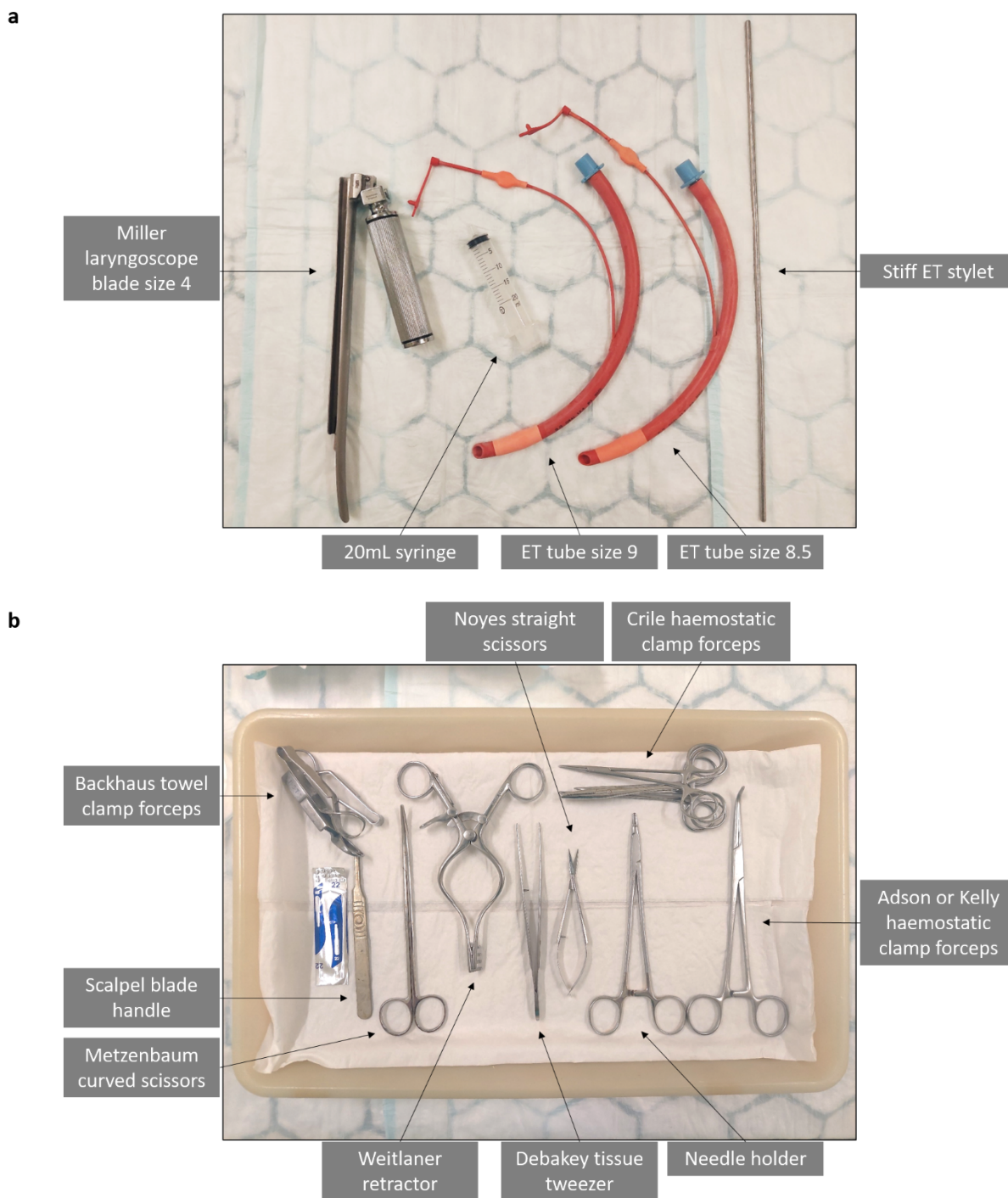
Fig. 13 – Typical surgical equipment. a, Intubation equipment. **b,** Surgical tray.

Operator preparation

- Surgical gown
- Surgical cap
- Sterile gloves
- Surgical face mask
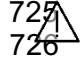- Radiation protective equipment – lead gown (Kenex, UK) and thyroid collar

Software

- ECG recording software details

Surgical procedure

A. Anaesthetic induction and preparation

⚠ Prior to surgery, animals are given access to water but food is witheld to avoid ruminal distension.

1. The animal is allowed to inhale a combination of oxygen and nitrous oxide in a 50:50 mix with isoflurane (3-5%).
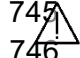
2. Animal is lifted and placed on the operating table in a sternal recumbency position, with the head elevated.

3. With the aid of a second operator, the jaw is opened with the head supported to allow the primary operator to spray two puffs of local anaesthetic (Lidocaine throat spray) into the back of the throat.

4. The facemask delivering oxygen nitrous 50:50 with isoflurane is replaced in preparation for intubation.

5. The facemask is removed and the jaw is held open with the head supported by the second operator. A laryngoscope is introduced and the vocal cords visualised.

6. A stiff stylet is taken down to the level of the vocal cords. An appropriately sized endotracheal tube is advanced over the stylet past the vocal cord and the stylet is removed. The cuff is inflated with air using a 20mL syringe and the tube is connected to a bag mask to confirm the appropriate tube placement in the trachea. The tube is then connected to the ventilator. The appropriate tube placement is confirmed by appropriate chest wall movement with the ventilator, saturation recordings, and the maintenance of anesthesia, and the tube is secured with the tie around the jaw.

⚠ When advancing stylet, due care is taken not to advance the stylet too far to avoid damage to soft tissue or larynx. Adequate visualisation of vocal cords is required to ensure safe placement.

7. The animal was positioned in lateral recumbency for the rest of the procedure.

8. All monitoring equipment (saturations monitoring, ECG monitoring, and BP monitoring) is connected.

9. A 20G cannula is sited on the right hind leg for the purposes of administration of intraoperative medications. Pre-operative antibiotics and analgesia are administered at this stage.
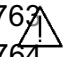
10. The right side of the neck is shaved, providing a wide surgical field.

11. The skin is cleaned twice with an iodine-based antiseptic and draped.

12. Anatomical landmarks are palpated to delineate the jugular groove.

27

13. A 5 to 7cm incision is made to the skin with a blade within the jugular grove. The incision site is located two thirds of the way from the angle of the jaw to the shoulder tip. This is followed by blunt dissection down to identify the jugular vein.

14. The jugular vein is identified and freed. A proximal and distal 2.0 silk suture is placed loosely on the vessel. These ties are clipped onto the drapes using the Crile (?artery) forceps.
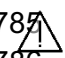
⚠ Gentle dissection is performed to free the jugular vein and carotid artery to avoid vascular damage. The vagal nerve must be gently freed from the carotid artery.

15. Further blunt dissection is performed deeper to identify the carotid artery, which runs alongside the vagus nerve. The carotid artery is freed from the vagus nerved and similar proximal and distal 2.0 silk sutures are placed and clipped to the drape loosely.

The procedure is carried out in two phases. The first stage involves implantation of an internal cardiac defibrillator to manage intraoperative life-threatening ventricular arrhythmias and the second stage is the induction of MI.

B. Implantation of an internal cardiac defibrillator (ICD)

1. The proximal jugular vein suture is tied off.
2. The mobile C-arm of the fluoroscopy machine is moved into position over the heart in the postero-anterior position.
3. With Noyes scissors, a venotomy is performed, exposing the inner lumen of the vessel.
4. With the aid of a vein pick, the vein is kept open and an active fixation RV lead, with a straight stylet in position, is advanced down to the right ventricular apex under fluoroscopy guidance. Due caution is taken when advancing the lead and lead advancement is stopped if there is any resistance.
5. As the lead crosses the tricuspid valve and is advanced into the RV, the ECG is monitored for the presence of ventricular ectopics suggestive of crossing the valve into the RV.

⚠ Advancement of the lead is performed cautiously across the tricuspid valve. If the lead does not directly cross the valve, the lead is prolapsed with the stylet retracted ~5cm - 8cm followed by straightening out the lead with the stylet fully inserted.

6. Once at the RV apex, the active fixation lead is deployed by applying clockwise turns on the proximal end of the lead to screw in the lead.
7. With the analyser connected to the distal end of the lead, the lead parameters are tested in the bipolar configuration. Target parameters include an R wave > 6mV, an impedance value between 300–1500Ω and a pacing threshold of <1V.
8. The lead is secured with 2.0 silk ties at the proximal and distal lead cuffs. The distal cuff is secured with the jugular vein simultaneously achieving vein closure and haemostasis.
9. The lead is connected to the appropriate port of the generator.

10. The subcutaneous pocket for the generator is created. The site needs to be sufficiently distal to the original incision towards the shoulder. The generator with the residual lead coiled is placed into the pocket.
11. The pocket is closed with interrupted 2.0 Vicryl sutures.
12. The VT, VF and FVT zones are programmed for detection only and all therapy is turned off. The rationale behind this is to avoid inappropriate shocks as the higher sinus rates and T wave oversensing in the model.
13. The device is then left connected wirelessly to the programmer in the emergency mode to allow prompt defibrillation of intra-operative life-threatening ventricular arrhythmias.

C. Induction of myocardial infarction

All the MI induction equipment (except the indeflator and the balloon) listed above should be pre-flushed with heparinised saline solution (i.e., 500mL sodium chloride 0.9% solution containing 10,000 IU heparin prepared in a sterile kidney dish) and prepared as follows:

- Insert the dilator into the 6 Fr haemostatic introducer sheath.
- Connect the 6F JR4 guide catheter to the Honor® Hemostasis Valve, which is connected to a 3-way valve, and then insert the 0.35 J tipped guide wire through the Hemostasis Valve all the way to the end of the catheter.

1. The previously identified carotid artery is the vascular access site for this part of the procedure.
2. The proximal suture is tied off.
3. The vessel is controlled with the previously placed proximal and distal ties.
4. A 14G cannula is advanced into the carotid artery towards the distal end.

The cannula is cautiously inserted to remain intraluminal and avoid transecting the carotid artery.

5. Once intravascular access is achieved, the x short guide wire is advanced down the cannula and exchanged for the 6F 12cm haemostatic sheath using the Seldinger technique.
6. The sheath is loosely secured via the side loop to prevent displacement secondary to the carotid pulsation.
7. Upon achieving arterial access, a 10,000 IU bolus if IV heparin is administered followed by a maintenance infusion of 10IU/ml to reduce the risk of thrombotic complications with the indwelling arterial equipment.
8. 30 minutes prior to coronary access, amiodarone 100mg IV is administered followed by a maintenance bolus dose of 50mg/hour.
9. Via the introducer sheath, a 6F Guide Judkins Right (JR4) catheter is advanced with a pre-loaded wire 0.35 in 150cm J wire. This is introduced under fluoroscopic guidance with the J wire leading to reduce vascular trauma.
10. The J wire is advanced down to the aortic valve. When it reaches the aortic valve, mild resistance should be felt, which corresponds to the J wire looping at the valve level.
11. Then the guide catheter is advanced over the wire down to the aortic valve level and the wire is removed.

843   12. A 50ml syringe with 50% contrast mix is connected to the end of the guide catheter.

844   13. Using fluoroscopic guidance, the catheter is advanced into the left coronary system

845   with catheter motion and contrast injection used to confirm/identify position.

846 ⚠   Engagement of left coronary artery system is done gently under direct fluoroscopic

847   guidance observing catheter tip motion and a gentle contrast injection to ensure the

848   ostium of the vessel is not dissected and to avoid deep intubation of the coronary.

849   14. Once engaged adequately, coronary angiography is performed with the 50% contrast

850   mixture to delineate the left coronary anatomy identifying the LAD coronary artery and

851   the second diagonal branch (D2). This will guide identification of the occlusion target

852   which is in the LAD after the D2 branch.

853   15. A bolus dose of 100mg Lidocaine is administered intravenously 20-30 minutes prior to

854   coronary occlusion via the peripheral cannula.

855   16. Coronary engagement is maintained with the guide catheter, whilst a 0.0014 in wire

856   (normal length wire) is advanced down to the distal LAD. The wire is introduced into

857   the haemostasis valve via the introducer needle provided in the set.

858 ⚠   The wire is advanced gently under fluoroscopic guidance to avoid coronary

859   perforation. Avoid buckling the wire tip as it is advanced.

860   17. The indeflator is prepared with the 50:50 contrast and heparinised saline solution mix.

861   For this, the chamber of the indeflator is filled with the mixture by aspiration, then the

862   handle is turned clockwise to expulse the fluid, removing any leftover bubbles and

863   leaving the mixture bubble-free.

864   18. Depending on the approximated diameter of the vessel (which is determined by

865   comparing the vessel calibre to the guide catheter, which represents a width of

866   approximately 2 mm), an appropriate size intracoronary balloon is selected.

867   19. The balloon's chamber is filled with contrast to ensure there is no air and is connected

868   to the indeflator. A vacuum is created by adding negative pressure and holding it in

869   place to empty the balloon and ensuring that there is no air within. The vacuum must

870   be maintained during the balloon's introduction.

871

872 ⚠   Ensure that the device is undamaged.

873   Do not pre-inflate or test the balloon before insertion.

874

875   20. The protective sleeve is removed from the balloon. The balloon catheter has a central

876   lumen, which allows it to be advanced over the 0.0014 in wire.

877   21. The 0.0014 in wire is fixed in the distal LAD and the intracoronary balloon is advanced

878   to the target site of occlusion over this wire whilst maintaining the distal position of this

879   wire at all times.

880 ⚠   As the balloon is advanced, it is critical to hold in place the thin wire, so it does not

881   cause coronary trauma or perforation by inadvertent advancement.

882

883   22. The indeflator is used to inflate the intracoronary balloon at the target occlusion point

884   within the LAD (i.e., immediately after the D2 vessel bifurcates). The contrast mixture

885   is filled into the intracoronary balloon by the indeflator, resulting in the occlusion.

886
887 ⚠ Inflation of the intracoronary balloon is performed slowly to ensure adequate but not excessive inflation which can cause coronary artery damage.

888 23. A coronary angiogram is performed to confirm that there is no visible flow of contrast
889 distal to the occlusion point suggesting adequate balloon inflation and this inflation is
890 maintained for a 90-minute duration.
891 24. A further bolus intravenous dose of 50mg Lidocaine is administered via the peripheral
892 cannula at 20 minutes post occlusion.

893
894 ⚠ Continuous monitoring of ECG, blood pressure, and oxygen saturations are necessary during this time.

895

896 25. Typically, animals begin to show ST changes almost immediately after the occlusion,
897 with ventricular arrhythmias happening between 20-40 minutes later. Any ventricular
898 arrhythmias need to be quickly treated by internal cardiac defibrillation using the 35J
899 cardiac defibrillator device that has been implanted in the beginning of the procedure.
900 This is done manually, using the header of the ICD programmer, since the device is in
901 emergency mode.
902

903
904 ⚠ Prompt defibrillation is necessary upon recognition of ventricular arrhythmia. This
905 may sometimes require multiple defibrillations. Therefore it is important to ensure that the implanted device has sufficient battery life.

906
907 26. Coronary perfusion is restored by deflation of the balloon at 90 minutes with a coronary
908 angiogram confirming re-perfusion down the coronary artery.
909 27. Atenolol 1mg is administered intravenously via the peripheral cannula on reperfusion.
910 28. The guide, balloon and wire are removed from the heart.
911 29. The carotid sheath is removed and the carotid artery is tied off with a 2.0 silk suture
912 achieving haemostasis.

913
914 ⚠ The removal of the carotid sheath is performed simultanously as the carotid is tied off to avoid excessive bleeding.

915

916 30. The wound is closed in layers with a 2.0 monocryl absorbable suture.
917 31. The animal is then gradually awakened, extubated, and recovered.
918 32. The animal is checked one hour after recovering from the procedure. Observations are
919 made from a safe distance to confirm that it is still alive, aware, and moving around in
920 the pen.
921 33. On the first day, any interaction with the animal is limited to prevent frightening it and
922 arrhythmias.
923

Reference

1. Bhatnagar, P., Wickramasinghe, K., Williams, J., Rayner, M. & Townsend, N. The epidemiology of cardiovascular disease in the UK 2014. *Heart* **101**, 1182-1189 (2015).
2. BHF (2022).
3. Organization, W.H. World health statistics 2016: monitoring health for the SDGs sustainable development goals. (World Health Organization, 2016).
4. Sawyer, D.B. & Vasan, R.S. Encyclopedia of Cardiovascular Research and Medicine. (Elsevier, 2017).
5. Ambrose, J.A. & Singh, M. Pathophysiology of coronary artery disease leading to acute coronary syndromes. *F1000Prime Rep* **7**, 08 (2015).
6. Fuster, V. Lewis A. Conner Memorial Lecture. Mechanisms leading to myocardial infarction: insights from studies of vascular biology. *Circulation* **90**, 2126-2146 (1994).
7. Saleh, M. & Ambrose, J.A. Understanding myocardial infarction. *F1000Res* **7** (2018).
8. Reimer, K.A., Lowe, J.E., Rasmussen, M.M. & Jennings, R.B. The wavefront phenomenon of ischemic cell death. 1. Myocardial infarct size vs duration of coronary occlusion in dogs. *Circulation* **56**, 786-794 (1977).
9. Sarafoff, N. et al. Association of ST-elevation and non-ST-elevation presentation on ECG with transmurality and size of myocardial infarction as assessed by contrast-enhanced magnetic resonance imaging. *J Electrocardiol* **46**, 100-106 (2013).
10. Greulich, S. et al. Time-Dependent Myocardial Necrosis in Patients With ST-Segment-Elevation Myocardial Infarction Without Angiographic Collateral Flow Visualized by Cardiac Magnetic Resonance Imaging: Results From the Multicenter STEMI-SCAR Project. *J Am Heart Assoc* **8**, e012429 (2019).
11. Collet, J.P. et al. 2020 ESC Guidelines for the management of acute coronary syndromes in patients presenting without persistent ST-segment elevation. *Eur Heart J* **42**, 1289-1367 (2021).
12. UK, N.C.G.C. Myocardial Infarction with ST-Segment Elevation: The Acute Management of Myocardial Infarction with ST-Segment Elevation [Internet]. (2013).
13. Goldman, L. & Schafer, A.I. Goldman's cecil medicine E-book. (Elsevier Health Sciences, 2011).
14. Bhar-Amato, J., Davies, W. & Agarwal, S. Ventricular Arrhythmia after Acute Myocardial Infarction: 'The Perfect Storm'. *Arrhythm Electrophysiol Rev* **6**, 134-139 (2017).
15. Torabi, A. et al. The timing of development and subsequent clinical course of heart failure after a myocardial infarction. *Eur Heart J* **29**, 859-870 (2008).
16. Takada, T. et al. Impact of Late Ventricular Arrhythmias on Cardiac Mortality in Patients with Acute Myocardial Infarction. *J Interv Cardiol* **2019**, 5345178 (2019).
17. Cahill, T.J. & Kharbanda, R.K. Heart failure after myocardial infarction in the era of primary percutaneous coronary intervention: Mechanisms, incidence and identification of patients at risk. *World J Cardiol* **9**, 407-415 (2017).
18. Henkel, D.M. et al. Ventricular arrhythmias after acute myocardial infarction: a 20-year community study. *Am Heart J* **151**, 806-812 (2006).

19. Camacho Londoño, J.E. et al. A background Ca2+ entry pathway mediated by TRPC1/TRPC4 is critical for development of pathological cardiac remodelling. *Eur Heart J* **36**, 2257-2266 (2015).

20. Spata, T. et al. A nonthoracotomy myocardial infarction model in an ovine using autologous platelets. *Biomed Res Int* **2013**, 938047 (2013).

21. Kim, Y.K. et al. Altered excitation-contraction coupling in myocytes from remodeled myocardium after chronic myocardial infarction. *JMCC* **34**, 63-73 (2002).

22. Hegyi, B. et al. Complex electrophysiological remodeling in postinfarction ischemic heart failure. *Proc Natl Acad Sci U S A* **115**, E3036-e3044 (2018).

23. Dardenne, A. et al. Benefits of standardizing the treatment of arrhythmias in the sheep (Ovis aries) model of chronic heart failure after myocardial infarction. *J Am Assoc Lab Anim Sci* **52**, 290-294 (2013).

24. Dib, N. et al. A percutaneous swine model of myocardial infarction. *J Pharmacol Toxicol Methods* **53**, 256-263 (2006).

25. Riehle, C. & Bauersachs, J. Small animal models of heart failure. *Cardiovascular Research* **115**, 1838-1849 (2019).

26. Sattler, S.M. et al. Ventricular Arrhythmias in First Acute Myocardial Infarction: Epidemiology, Mechanisms, and Interventions in Large Animal Models. *Frontiers in Cardiovascular Medicine* **6** (2019).

27. Ibanez, B. et al. 2017 ESC Guidelines for the management of acute myocardial infarction in patients presenting with ST-segment elevation: The Task Force for the management of acute myocardial infarction in patients presenting with ST-segment elevation of the European Society of Cardiology (ESC). *Eur Heart J* **39**, 119-177 (2017).

28. Ikram, H. et al. An ovine model of acute myocardial infarction and chronic left ventricular dysfunction. *Angiology* **48**, 679-688 (1997).

29. Bowen, F.W. et al. Reappearance of myocytes in ovine infarcts produced by six hours of complete ischemia followed by reperfusion. *Ann Thorac Surg* **71**, 1845-1855 (2001).

30. eBioMedicine The 3Rs of Animal Research. *EBioMedicine* **76**, 103900 (2022).

31. Percie du Sert, N. et al. in PLoS Biol, Vol. 18 (2020).

32. Lee, K.H., Lee, D.W. & Kang, B.C. The 'R' principles in laboratory animal experiments. *Lab Anim Res* **36**, 45 (2020).

33. Houser, S.R. et al. Animal models of heart failure: a scientific statement from the American Heart Association. *Circ Res* **111**, 131-150 (2012).

34. Piktel, J.S. & Wilson, L.D. Translational Models of Arrhythmia Mechanisms and Susceptibility: Success and Challenges of Modeling Human Disease. *Frontiers in Cardiovascular Medicine* **6** (2019).

35. Shin, H.S., Shin, H.H. & Shudo, Y. Current Status and Limitations of Myocardial Infarction Large Animal Models in Cardiovascular Translational Research. *Front Bioeng Biotechnol* **9**, 673683 (2021).

36. Flameng, W., Schwarz, F. & Schaper, W. Coronary collaterals in the canine heart: development and functional significance. *Am Heart J* **97**, 70-77 (1979).

37. Munz, M.R., Faria, M.A., Monteiro, J.R., Aguas, A.P. & Amorim, M.J. Surgical porcine myocardial infarction model through permanent coronary occlusion. *Comp Med* **61**, 445-452 (2011).

38. Milani-Nejad, N. & Janssen, P.M. Small and large animal models in cardiac contraction research: advantages and disadvantages. *Pharmacol Ther* **141**, 235-249 (2014).

1022 39. Daubert, M.A. & Jeremias, A. The utility of troponin measurement to detect
1023 myocardial infarction: review of the current findings. *Vasc Health Risk Manag*
1024 **6**, 691-699 (2010).
1025 40. Thygesen, K. et al. Third universal definition of myocardial infarction. *Eur*
1026 *Heart J* **33**, 2551-2567 (2012).
1027 41. Thygesen, K. et al. Fourth Universal Definition of Myocardial Infarction (2018).
1028 *J Am Coll Cardiol* **72**, 2231-2264 (2018).
1029 42. Leonardi, F. et al. Cardiac Troponin I (cTnI) concentration in an ovine model
1030 of myocardial ischemia. *Res Vet Sci* **85**, 141-144 (2008).
1031 43. Maynard, S.J., Menown, I.B. & Adgey, A.A. Troponin T or troponin I as
1032 cardiac markers in ischaemic heart disease. *Heart* **83**, 371-373 (2000).
1033 44. Dasgupta, A. & Wahed, A. Clinical chemistry, immunology and laboratory
1034 quality control: a comprehensive review for board preparation, certification
1035 and clinical practice. (2013).
1036 45. Morrow, D.A. et al. National Academy of Clinical Biochemistry Laboratory
1037 Medicine Practice Guidelines: Clinical characteristics and utilization of
1038 biochemical markers in acute coronary syndromes. *Circulation* **115**, e356-375
1039 (2007).
1040 46. Mahajan, V.S. & Jarolim, P. How to interpret elevated cardiac troponin levels.
1041 *Circulation* **124**, 2350-2354 (2011).
1042 47. Marti-Carvajal, A.J., Simancas-Racines, D., Anand, V. & Bangdiwala, S.
1043 Prophylactic lidocaine for myocardial infarction. *Cochrane Database Syst Rev*,
1044 Cd008553 (2015).
1045 48. Locatelli, P. et al. An ovine model of postinfarction dilated cardiomyopathy in
1046 animals with highly variable coronary anatomy. *ILAR journal* **52**, E16-21
1047 (2011).
1048 49. Hassell, M.E. et al. Long-term left ventricular remodelling after
1049 revascularisation for ST-segment elevation myocardial infarction as assessed
1050 by cardiac magnetic resonance imaging. *Open Heart* **4**, e000569 (2017).
1051 50. Sutton, M.G. & Sharpe, N. Left ventricular remodeling after myocardial
1052 infarction: pathophysiology and therapy. *Circulation* **101**, 2981-2988 (2000).
1053 51. Rechavia, E. et al. Hyperdynamic performance of remote myocardium in
1054 acute infarction. Correlation between regional contractile function and
1055 myocardial perfusion. *Eur Heart J* **16**, 1845-1850 (1995).
1056 52. Latini, R., Tognoni, G. & Kates, R.E. Clinical pharmacokinetics of amiodarone.
1057 *Clin Pharmacokinet* **9**, 136-156 (1984).
1058 53. Li, T. et al. Prophylactic amiodarone and lidocaine improve survival in an
1059 ovine model of large size myocardial infarction. *J Surg Res* **185**, 152-158
1060 (2013).
1061 54. Deshpande, A. & Birnbaum, Y. ST-segment elevation: Distinguishing ST
1062 elevation myocardial infarction from ST elevation secondary to nonischemic
1063 etiologies. *World J Cardiol* **6**, 1067-1079 (2014).
1064 55. Okada, J.I. et al. Ionic mechanisms of ST segment elevation in
1065 electrocardiogram during acute myocardial infarction. *J Physiol Sci* **70**, 36
1066 (2020).
1067 56. Di Diego, J.M. & Antzelevitch, C. Acute myocardial ischemia: cellular
1068 mechanisms underlying ST segment elevation. *J Electrocardiol* **47**, 486-490
1069 (2014).

1070   57.   Pfeffer, M.A. & Braunwald, E. Ventricular remodeling after myocardial
1071   infarction. Experimental observations and clinical implications. *Circulation* **81**,
1072   1161-1172 (1990).
1073   58.   Litwin, S.E., Katz, S.E., Morgan, J.P. & Douglas, P.S. Serial
1074   echocardiographic assessment of left ventricular geometry and function after
1075   large myocardial infarction in the rat. *Circulation* **89**, 345-354 (1994).
1076   59.   Pennock, G.D., Yun, D.D., Agarwal, P.G., Spooner, P.H. & Goldman, S.
1077   Echocardiographic changes after myocardial infarction in a model of left
1078   ventricular diastolic dysfunction. *Am J Physiol* **273**, H2018-2029 (1997).
1079   60.   Galli, A. & Lombardi, F. Postinfarct Left Ventricular Remodelling: A Prevailing
1080   Cause of Heart Failure. *Cardiol Res Pract* **2016**, 2579832 (2016).
1081   61.   Sutton, M.G.S.J. & Sharpe, N. Left Ventricular Remodeling After Myocardial
1082   Infarction. *Circulation* **101**, 2981-2988 (2000).
1083   62.   Rubin, S.A., Fishbein, M.C. & Swan, H.J. Compensatory hypertrophy in the
1084   heart after myocardial infarction in the rat. *J Am Coll Cardiol* **1**, 1435-1441
1085   (1983).
1086   63.   Siddiqui, B.A. & Kim, P.Y. in StatPearls (StatPearls Publishing
1087   Copyright © 2022, StatPearls Publishing LLC., Treasure Island (FL); 2022).
1088   64.   Kleemann, T. et al. 96-42: Comparison of lead failure rates between DF-1 and
1089   DF-4 ICD leads in clinical practice. *EP Europace* **18**, i71-i71 (2016).
1090   65.   Rajappan, K. Permanent pacemaker implantation technique: part II. *Heart* **95**,
1091   334-342 (2009).
1092   66.   Swerdlow, C.D. et al. Impedance in the Diagnosis of Lead Malfunction. *Circ
1093   Arrhythm Electrophysiol* **13**, e008092 (2020).
1094   67.   Seldinger, S.I. Catheter replacement of the needle in percutaneous
1095   arteriography; a new technique. *Acta radiol* **39**, 368-376 (1953).

1096